RSC Advances

ROYAL SOCIETY OF CHEMISTRY

www.rsc.org/advances

The influence of nanofillers migration to the mechanical property of PA6/chitosan nanocomposites

Qi Zhou[1*], Jueyuan Zhang[1], Jianghua Fang[1], Wei Li[2]

[1]Department of Chemical Engineering, Ningbo University of Technology, Ningbo 315016, PR China

[2]Ningbo Key Laboratory of Special Polymer, Department of Polymer Science and Engineering, School of Material Science and Chemical Engineering, Ningbo University, Ningbo, 315211, Zhejiang. P. R. China

Corresponding authors:

Qi Zhou, E-mail address: zhouqi@nbut.cn

Abstract

Blends of chitosan (CS) with polyamide 6 (PA6) were prepared via the solution casting technique using formic acid as a common solvent. Polyhedral oligomeric silsesquioxane (POSS), montmorillonite (PGN), and modified montmorillonite (TCN and TL) were incorporated into the polymer matrix. The dispersion state of the nanofillers in the polymer matrix was characterized by polarized optical microscopy (POM), attenuated total reflection with flourier transformed infrared spectroscopy (FTIR-ATR), X-ray diffraction measurements (XRD) and transmission electron microscopy (TEM). It was shown that POSS could achieve the best dispersion state in the polymer matrix with only several tens of nanometers. Thermal and mechanical properties of the synthesized polymer nanocomposites were studied by differential scanning calorimetry (DSC) and Instron single column materials testing system. The morphology and element analysis of the cross-section of the sample film was characterized by scanning electron microscopy with energy dispersive X-ray (SEM/EDX) to further explain the mechanical property results. It was shown CS tended to sediment during the solvent evaporation step whereas PA6 rich domain fills upper zones of the samples. Interestingly, POSS was prior to migrate to the upper zone of PA6 rich domain, while PGN, TCN and TL prefered to migrate to the CS rich domain. The migration of nanofillers was found to be very important to improve the tensile strength of PA/CS belnds.

Keywords: PA6/CS nanocomposites; migration; POSS; mechanical properties.

1. Introduction

Phase inversion is a process by which a polymer is transformed from a liquid or soluble state to a solid state [1]. Phase inversion procedure is the most versatile technique with which to prepare polymeric membranes. A variety of morphologies can be obtained that are suitable for different applications, from microfiltration membrane with very porous structures, to more dense reverse osmosis membranes, to gas separation and pervaporation membranes, with a complete defect-free structure[2-3].

Chitosan (CS) is one of the most abundant polysaccharides found in nature [4,5]. This material has good solubility in the formic acid and can be synthesized to membrane according phase inversion process. Modification of CS by means of blending nylon was a convenient and effective method of improving physical properties for practical utilization. Films of chitosan-nylon-4 blends showed good mechanical properties and retain the excellent chelating ability of chitosan [6]. Blends of chitosan with strongly crystalline polyamides (nylon-4 and nylon-6) were also investigated. Their results suggested partial miscibility of chitosan with nylon-4 and lack of miscibility in other polyamides [7]. Dufresne A [8] had synthesized blends of chitosan with PA6 via phase inversion technique using formic acid as a common solvent. Due to the different density of PA6 and CS, CS phase tended to sediment and to form a continuous phase on the lower face of the film. The PA6 rich domains filled the upper face of the sample. A similar observation was reported for thermoplastic nanocomposites filled with wheat straw cellulose whiskers [9], and the behavior of

these materials was modeled by subdividing the sample into layers with different whiskers content, lying parallel to the film surface. This sedimentation phenomenon was of great importance to the mechanical behavior of the blend.

Incorporation of small amount of inorganic nanofillers during the formation of polymer membrane can endow the polymer new and much more improved mechanical, thermal and electrical properties [10, 11]. Recently, the migration behavior of nanofillers to the surface of polymer nanocomposites (PNCs) has attracted interest. This phenomenon has been reported to be greatly correlated to the preparation method of PNCs, especially during the phase inversion procedure [12, 13]. The migration of POSS [14] and MMT [15] was reported in PA6 [14], polypropylene [16] and polystyrene [17] synthesized by melting blend. Decreased surface free energy was considered to be the critical issue for the migration [16, 17]. Our group had studied the migration behaviors of POSS in the POSS/PA6 nanocomposites during phase inversion process [18]. It was found that octaammonium POSS (OA-POSS) had the greatest migration behaviors compared with other functional POSS. We suggested that strong interaction between nanofiller and polymer matrix was another important issue for the migration behaviors of nanofiller, including the surface free energy. Increase the interaction between nanofiller and polymer matrix could hinder the aggregation of filler which would improve the migration behavior of filler. However, it shall be mention that there is no publication focused on the migration of nanofiller in polymer blends with sedimentation structure, neither on the using performance thereof.

In this work, blends of CS with PA6 were prepared via the phase inversion process.

Four kinds of nanofiller were introduced into the polymer matrix, including POSS, polymer grade montmorillonite (PGN), bis(2-hydroxyethy)methyl tallow ammonium modified MMT (TCN) and 12-aminododecyl acid modified MMT (TL). The phase structure and morphology of chitosan/PA6 nanocomposites were studied. In particularly, the migration behaviors of nanofiller in the PA6/CS blends are characterized. We aim to know the influence of migration of nanofiller on the mechanical properties of polymer blends.

2. Experiments

2.1 Materials

PA6 pellets (M_w=30,000g/mol) and CS ($(C_6H_{11}NO_4)N$) were purchased from Sigma-Aldrich. The samples were dried in a vacuum oven for more than 24 h at 80˚C and then stored in a desiccator before usage. Octaammonium POSS (POSS), PGN: polymer grade montmorillonite, TCN: bis(2-hydroxyethy)methyl tallow ammonium modified MMT, TL: 12-aminododecyl acid modified MMT were purchased from hybrid plastics company. The density of PA6, chitosan, POSS and PGN is 0.89 g/cm^{-3}, 1.75 g/cm^{-3}, 1.40 g/cm^{-3} and 2.5 g/cm^{-3}, respectively. Figure 1 shows the structure of POSS and PGN. All the nanofillers were dried in a vacuum oven for more than 24h at 60 ˚C separately and then stored in a desiccator. Formic acid was purchased from Sigma-Aldrich with a purity of 99.5% and was used as received.

2.2 Preparation of PA6/ chitosan nanocomposites

The nanocomposites were synthesized by a solution-casting method. First, PA6 and chitosan were dissolved in formic acid (1 wt. %) for at least 24 h (1.0 g of PA6 in 20

ml of formic acid). Nanofillers were then added to the solution and stirred for at least 48 h. The appropriate amount of POSS was measured in order to form polymer nanocomposites with final compositions of 2 wt. %. After mixing, the mixture was transferred into an ultra-plate watch-glass and maintained at 40 °C. The glass substrate with sample films was left in the fume hood overnight to allow the formic acid solvent to evaporate. All the films were then dried in a vacuum oven at 80 °C for more than 12 h and subsequently kept in a desiccator before use.

2.3 Characterization

2.3.1 X-ray diffraction measurements (XRD)

XRD measurements were carried out on a Bruker GADDS diffractometer with an area detector operating under 40 kV and 40 mA, using Cu K_α radiation (λ= 0.154 nm).

2.3.2 Polarized optical microscopy (POM)

Surface morphology was analyzed by polarized optical microscopy (POM, BX51, OLYMPUS) at room temperature. The lens magnification was 10×.

2.3.3 Scanning electron microscopy (SEM) and Energy dispersive X-ray (EDX)

The morphology of the surfaces and cross sections of the films were analyzed by a HITACHI S-4800 scanning electron microscope using an acceleration voltage of 10 keV. Samples were put into the liquid nitrogen for several minutes, and were then snapped into half to obtain the cross section. EDX analysis was also conducted on the same instrument using the EDX apparatus.

2.3.4 Transmission election microscopy (TEM)

TEM (Tecnai F20, USA) was used to measure the morphology of the samples. Samples were cut by a freezing microtome before analyzed by the TEM.

2.3.5 Differential scanning calorimetry (DSC)

The heat enthalpy, melting point and glass transition temperature of PA6 and its nanocomposites were measured by a differential scanning calorimeter (Paris 1, PerkinElmer Co., Norwalk, CT) in a nitrogen atmosphere. The samples were analyzed by the following temperature program: heating from 50°C to 260°C at 10°C /min; maintaining for 3 min at 260°C; cooling to 50°C at 10°C /min; maintaining at 50°C for another 3 min before heating up again to 260°C at 10°C /min.

2.3.6 Tensile test

The tensile properties of the membranes were measured by an Instron model 5543 single column materials testing system. Films with a gauge length of 40 mm, width of 10 mm were stretched at a crosshead speed of 2 mm/min at 20 °C. The resulting data were taken from the average of at least five samples.

2.3.7 Attenuated total reflectance infrared resonance (ATR)

ATR spectroscopy was performed on a Nicolet Nexus spectrometer. The detector is a liquid nitrogen cooled mercury cadmium telluride (MCT) with a range of 650-4000 cm^{-1}. The resolution was 4 cm^{-1}.

3. Results and Discussions

3.1 Dispersion state of nanofillers in PA6/CS matrix

The miscibility of PA6 and CS will be greatly changed due to their different crystalline behaviors. Figure 2 shows that PA6/CS blends with 50 wt% of PA6 can achieve totally transparent morphology, indicating the uniform dispersion of PA6/CS blends can be achieved. This can be attributed to the improved co-crystallization behaviors between PA6 and CS. Hence, the PA6/CS nanofiller nanocomposites are synthesized based on this weight ratio.

POM is an effective way to observe the dispersion state of nanofiller in polymer matrix [19]. It is observed that PA6/CS-POSS nanocomposites have homogeneous surface morphology, as shown in Figure 3b. This indicates that the POSS particles are uniformly dispersed in the polymer matrix. Furthermore, the presence of large black domains indicative of nanofiller aggregates can be clearly observed on the surface of PA6/CS-PGN, PA6/CS-TCN and PA6/CS-TL nanocomposites (Figure 3 c, d, e). It can be attributed to the worse miscibility between clay and polymer matrix.

Figure 4 shows the XRD spectra of PA6/CS and its nanocomposites with different nanofillers. It is shown that two main peaks are observed at 20.5° and 24°, indicating that the morphology of the films is mainly α-crystals in all of the nanocomposites [20]. Moreover, the peak ranging from 4° to 8° is generated by the aggregation of nanofillers. In PA6/CS-POSS nanocomposites, there is no obvious peak in this region, indicating the POSS is exfoliated. It may be due to the similar solubility parameters between POSS and polymer matrix [18]. However, the peak ranging from 4° to 8° can

be found in PA6/CS-PGN nanocomposites, suggesting that the aggregators of PGN is notable. Moreover, the peak ranging from 4° to 8° is difficult to be found in the PA6/CS-TCN and PA6/CS-TL nanocompoistes. It indicates that TCN and TL can achieve good dispersion state in the polymer matrix [15, 18]. This may be due to the reason that modification of PGN by ammonium and 12-aminododecyl acid increase the interaction between clay and polymer matrix, through the enhanced interface interactions.

TEM images are further used to investigate the dispersion state of nanofiller in the polymer matrix (Figure 5). It is shown that POSS does achieve the best dispersion state in the PA6/CS matrix with only several tens of nanometers. This shows great correspondence with that of XRD results. However, the aggregator of PGN in the polymer matrix is larger in size. This is the reason for a new diffraction peak generated from 4° to 8° in the XRD spectra. After chemical modification of PGN, the introduction of amino, hydroxyl and acid group increases the interface interaction between nanoparticles (TCN and TL) and polymer matrix. This will increase the miscibility between nanofiller and polymer matrix. Thus, the aggregator of nanofiller will decrease in size.

3.2 DSC characterization

Figure 6 shows the effects of the nanofiller additives on the crystallization behavior of PA6/CS membranes measured by DSC. A broad endotherm is observed around 90 °C which is the typical melting point of CS. [21, 22] In addition, all the samples have obvious melting point around 220 °C which is mainly generated by the α form

crystals of PA6. [21] The melting peak of CS phase changes indistinctly with the incorporation of PGN compared with PA6/CS blends. It can be attributed to the poor dispersion state of PGN in the polymer matrix. However, a gradually increase of melting peak of CS is shown with the incorporation of POSS, TCN and TL, indicating the intermolecular hydrogen bonds interaction between nanoparticles of CS are increased in the order of POSS, TCN and TL [22,23]. Table 2 shows the DSC data of PA6 phase. The variance of melting enthalpy upon the incorporation of nanoparticles is not obvious. Thus, it is difficult to discuss the influence of crystalline behaviors of nanocomposites generated by the incorporation of nanoparticles. However, the melting peaks and crystallization peaks (Figure 6 a, b) of nanocomposites are slightly increased in the PA6 phases when the nanoparticles are incorporated. It may be due to the mildly enhanced interface interactions between PA6 phase and nanoparticles.

3.3 Tensile properties

Figure 7 shows the tensile strength (Figure 7a) and breaking strains (7b) of the polymer nanocomposites. It is clearly observed CS has higher tensile strength and breaking strains than that of PA6. The tensile strength of PA6/CS nanocomposites are in between that of PA6 and CS. The inter-hydrogen bonds between chitosan and polyamide, which makes the molecules bind tightly, so the tensile strength increases compared with that of PA6 [24]. Interestingly, the breaking strains of PA6/CS obviously decrease. Further incorporations of nanoparticles (POSS, PGN, TGN and TL) lead to an increment of tensile strength and breaking strains compared with that of pure PA6/CS. The incorporation of nanoparticle into the PA6/CS matrix will

increase the interface interactions between nanoparticles and polymer matrix, resulting in an enhancement of stress transfer property. In addition, the exfoliated nanoparticles can also transfer the stress during the tensile process. Thus, the tensile property of nanocomposites is improved compared with that of PA6/CS blends.

However, the tensile strength and breaking strains decrease in the order of PA6/CS-POSS, PA6/CS-PGN, PA6/CS-TGN and PA6/CS-TL. It had been shown by the experiments and model studies that the high modulus and high aspect ratio of nanofillers could achieve good mechanical performance in pure PA6/nanofiller nanocomposites. In this work, PGN, TCN and TL are typical nanofillers with high modulus and high aspect ratio. The reinforcing efficiency should be increased if an exfoliated dispersion state can be achieved [25]. However, our results seem to be contradictory with the previous observation of dispersion state and DSC result. It shall be mentioned that the above study on the dispersion state of nanofillers (TEM, XRD and POM) is mainly characterized from the bulk of polymer matrix. Morphology of the polymer films, especially which along the thick direction, will be further studied.

3.4 Morphology studies

3.4.1 Dispersion of CS in the polymer matrix

Figure 8 shows the SEM images of PA6/CS and PA6/CS nanocomposites on the top and bottom side. The top side (Figure 8a) of PA6/CS appears as an undulating surface because of the evaporation process [8]. In contrast, the bottom face is scored (Figure 7a'), probably because of the surface effect of the box in which the blend solution is cast. The top face is still undulated with the incorporation of PGN. However, the top

face gradually turns to smooth in the order of PA6/CS-TCN, PA6/CS-TL and PA6/CS-POSS. This may indicates that the increased interaction between solvent, nanofiller and polymer matrix can influence the phase separation procedure.

Figure 9 shows images of the cross-section images of PA6/CS and PA6/CS nanocomoposites. It can be found that the polymer matrix is rather condensed and nonporous combined to the images of top and bottom side. Interestingly, the morphologies are different across the red line as shown in the image. The upper zone looks transversal, while the lower zone seems longitudinal. This is an indication that CS and PA6 in the blend form mainly a two-phase system. Dufresne A [8] had synthesized blends of chitosan with PA6 via the phase inversion process. They had found that CS phase tended to sediment and to form a continuous phase on the lower face of the film, while PA6 rich domains filled the upper face of the sample. Thus, the different morphologies across the red line may be due to the different polymer composition.

One of the main characteristics of PA or CS is the strong inter-chain interaction that arises from the hydrogen bonding between amide groups on adjacent chains. Generally, some nanofiller can form hydrogen bonds with amide groups at interfaces, which can be clearly characterized by ATR [22]. Figure 10 shows that the ATR spectra of the samples on top side and bottom side are quite different. In figure 10a, the ATR spectra of polymer on top side have more PA6 signal[26]: where the characteristic assignments of PA6 are 3300 cm^{-1} (sharp peak, H-bonded N-H stretch vibration), 3080 cm^{-1} (N-H in-plane bending), 1640 cm^{-1} (amide I, C=O stretch), 1540

cm^{-1}(amide II, C-N stretch and CO-N-H bend). In figure 10b, the ATR spectra of polymer on bottom side are more likely with CS [27, 28]. The absorption occurs around 898 and 1150 cm^{-1} are assigned to saccharine structure in CS. Bands at 1060 and 1029 cm^{-1} involve C=O stretching belongs to the CS as well. These indicate that the sedimentation of CS exist in the synthesized polymers. The lower face of the film seems to present CS rich domains. This gradient of CS concentration is probably induced by the processing technique itself. The CS domains tend to sediment during the solvent evaporation step. This phenomenon is due to the difference between the density of CS ($\rho \approx 1.75$) and that of PA6 ($\rho \approx 0.89$)[8].

In addition, the ATR spectra of PA6 rich phase and nanocomposites in the hydrogen-bonded N-H stretch region (3100-3400 cm^{-1}) shows little variance in the peak width. It indicates that the interface interaction between nanoparticles and PA6 rich phase is not strong [22]. However, the peak width of hydrogen-bonded N-H stretch region in the CS rich phase is obiously increased, indicating a strong interface interaction between nanoparticle and CS rich phase. This shows great coorespondence with the results of DSC.

3.4.2 Migration of nanofillers in the polymer matrix

Table 2 summaries the silicon atom content of polymer and polymer nanocomposites with different nanofiller qualitatively measured by EDX [18]. Typical selected zone for EDX is shown in Figure 11. One can image that the measured silicon atom content shall be close to each other in all the part if the dispersion of nanofillers is uniform in the three-dimension of the polymer matrix. However, these

contents, measured by EDX, are obvious different as is shown in Table 2. It can be found that the content of silicon atom is much higher on the cross-section upper zone and top side than the lower zone for PA6/CS-POSS. It indicates that POSS is prior to migrate to the top surface of the membrane during the phase inversion procedure [18]. This could be due to the less surface free energy and strong interaction between POSS and PA6 matrix [15, 18]. However, PGN, TCN and TL have shown an opposite migrating direction where much higher silicon concentration can be measured on the lower zone. In other words, the PGN, TCN and TL tend to migrate to the bottom side. This could be due to the large density of the PGN, TCN and TL (≈2.5 g/cm^{-3}). The density of PGN, TCN and TL is large than that of PA6 and CS. As a result, the PGN, TCN and TL are prior to sedimentation.

3.5 The influence of tensile strength generated by the migration of nanofiller

Figure 12 shows the proposed mechanism of the influence of migration of nanofiller to the tensile property. From the morphology studies, CS domains tend to sediment during the solvent evaporation step. PA6 rich domains fill the upper zone of the samples. This heterogenous distribution state will make the sample more easily break when a symmetric force is loading. As a result, decrease the variance of tensile strength between PA6 rich domains and CS rich domains is very important to improve the tensile strength of PA/CS belnds. The POSS is prior to migrate to the PA6 rich phase with good dispersion state. Thus, more nanparticles can be used to transfer the stress in the PA6 rich phase during the tensile measurement. These will increase the tensile strength and breaking strains of PA6 rich domains. The variance of mechaincal

properties between PA6 rich domains and CS rich domains is decreased thereof. Thus, the tensile strength and breaking strains of PA6/CS-POSS nanocomopsites is higher than that of PA6/CS blends. For the PA6/CS-clay systems, the mechanical properties of nanocomposites can be improved due to the good dispersion state of the clay in the PA6/CS matrix. However, the PGN, TCN and TL can achieve more loading in the CS rich domains. In addition, chemical modifation of PGN will increase the interface interaction between clay and CS rich phase, resulting in an increment of the tensile strength of CS rich domains. This will enlarge the variance of mechanical properties between PA6 rich domains and CS rich domains. Thus, the tensile strength and breaking strains gradually decreases in the order of PA6/CS-PGN, PA6/CS-TGN and PA6/CS-TL.

4. Conclusions

PA6/CS blended with POSS, PGN, TCN and TL nanocomposites are synthesized according to phase inversion procedure. The TEM, POM and XRD are used to characterize the dispersion state of nanofiller in the polymer matrix. The results show that POSS can be achieved the best dispersion state in the polymer matrix with only several tens of nanometers. Modification of PGN (TCN and TL) can improved the dispersion state of the nanofillers. However, the dispersion state results cannot well explain the results of tensile strength. Further study on the morphologies of polymer along the thick direction shows that: CS domains tend to sediment during the solvent evaporation step. PA6 rich domains filler upper zone of the samples. POSS is prior to migrate to the upper zone. The strong interaction between POSS and PA6 will

increase the tensile strength of PA6 rich domains. This makes the variance of mechainal properties between PA6 rich domains and CS rich domains decrease, resulting in an improved tensile strength of the polymer matrix entirety. PGN, TCN and TL are sediment to the CS rich phase which will resulting in an increased tensile strength of CS rich domains. This enlarges the variance of mechanical properties between PA6 rich domains and CS rich domains. The tensile strength of the polymer matrix entirety decreased when more strong interaction between nanofillers and CS rich domains occurred.

Acknowledements

Funding from the project of Natural Science Foundation of China (No. 51203081, 21206078), the Natural Science Foundation of Ningbo (2012A610087) and Ningbo Science and Technology Innovation Team (2011B2002) are gratefully acknowledged.

References

1. Lalia, B.S.; Kochkodan, V.; Hashaikeh, R.; Hilal, N. A review on membrane fabrication: Structure, properties and performance relationship. *Desalination*, **2013**, *326*, 77-95.
2. Venault, A.; Chang, Y.; Wang, D.M.; Bouyer, D. A Review on Polymeric Membranes and Hydrogels Prepared by Vapor-Induced Phase Separation Process, *Polymer Review*, **2013**, *53*, 568-626.
3. Guillen, G.R.; Pan, Y.J.; Li, M.H.; Hoek, E.M.V. Preparation and Characterization of Membranes Formed by Nonsolvent Induced Phase Separation: A Review. *Ind Eng Chem Res*, **2011**, *50*, 3798-3817.

4. Don, T.M.; Hu, Y.C.; Tai, H.Y.; Fu E, Cheng LP, Preparation of bi-continuous macroporous polyamide copolymer membranes for cell culture, *Journal of Membrane Science*, **2012**, *415*, 784-792.
5. Hong, H.; Wei, J.; Liu, C.S. Development of asymmetric gradational-changed porous chitosan membrane for guided periodontal tissue regeneration, *Composites Part B-Engineering*, **2007**, *38*, 311-316.
6. Kim, D.Y.; Ratto, J.A.; Blumstein, R.B. Investigation of the phase behavior for chitosan polyamide blends, *Polym Prepr* **1991**, *31*, 112.
7. Ratto, J.A.; Chen, C.C. Blumstein RB. Phase behavior study of chitosan polyamide blends. *J Appl Polym Sci* **1996**,*59*,1451.
8. Dureesne, A.; Cavaillé, J.Y.; Dupeyre. D.; Ramirez, M. G.; Romero, J. Morphology, phase continuity and mechanical behaviour of polyamide 6/chitosan blends. *Polymer*, **1999**, *40*, 1657-1666.
9. Dufresne, A.; Cavaillé, J.Y.; Helbert, W. Thermoplastic nanocomposites filled with wheat straw cellulose whiskers .2. Effect of processing and modeling, *Polym Compos,* **1997**, *18*,198-210.
10. Pavlidou, S.; Papaspyrides C.D. A review on polymer-layered silicate nanocomposites. *Prog. Polym. Sci.* **2008**, *33*, 1119-1198.
11. Paul, D.R.; Robeson, L.M. Polymer nanotechnology: nanocomposites. *Polymer*, **2008**, *49*, 3187-3204.
12. Gnanasekaran, D.; Madhavan, K.; Reddy, B.S.R.; Developments of polyhedral oligomeric silsesquioxanes (POSS), POSS nanocomposites and their applications:

a review. *J. Sci. Ind. Res.* **2009**, *68*, 37-464.

13. Cordes D.B.; Lickiss P.D.; Ratabou F. Recent developments in the chemistry of cubic polyhedral oligosilsesquioxanes. *Chem. Rev.* **2010**, *110*, 2081-2173.
14. Misra R.; Bruce F.X.; Plagge A.; Morgan S.E. POSS-nylon 6 nanocomposites: influence of POSS structure on surface and bulk properties. *J. Polym. Sci. Part B: Polym. Phys.* **2009**, *47*, 1088-1102.
15. Zhou, Q.; Wang K.; Loo L.S. Role of interface in dispersion and surface energetics of polymer nanocomposites containing hydrophilic POSS and layered silicates, *J. Colloid Interface Sci.* **2011**, *335*, 222-230.
16. Tang, Y.; Lewin, M. Migration and surface modification in polypropylene (PP)/polyhedral oligomeric silsequioxane (POSS) nanocomposites. *Polym Adv Technol* **2009**, *20*, 1-15.
17. Misra, R.; Alidedeoglu A.H.; Jarrett W.L.; Morgan S.E. Molecular miscibility and chain dynamics in POSS/polystyrene blends: control of POSS preferential dispersion states. *Polymer* **2009**, *50*, 2906-2918.
18. Zhou, Q.; Wang, Z.Q.; Shi, Y.L.; Fang, J.H.; Gao, H.Q.; Loo, L.S. The migration of POSS molecules in PA6 matrix during phase inversion process. *Appl Surf Sci* **2013**, *284*, 118-125.
19. Filippi, S.; Mameli E.; Marazzato C.; Magagnini P. Comparison of solution blending and melt-intercalation for the preparation of poly(ethyleneco-acrylic acid)/organoclay nanocomposite. *Eur Polym J* **2007**, *43*, 1645.
20. Zhou, Q.; Fang, J.H.; Gao, H.Q.; Loo, L.S. Substrate effects on the surface

properties of nylon 6. *Appl Surf Sci* **2013**, *282*, 115-120.

21. Zhang, H.T.; Li, S.B.; White, C.J.B.; Ning, X.; Nie, H.L.; Zhu, L.M. Studies on electrospun nylon-6/chitosan complex nanofiber interactions. *Electrochimica Acta* **2009**, *54*, 5739-5745.
22. Zhou, Q.; Pramoda K.P.; Lee J.M.; Wang K.; Loo L.S. Role of interface in dispersion and surface energetic of polymer nanocomposites containing hydrophilic POSS and layered silicates. *Journal of Colloid and Interface Science* **2011**, *355*, 222-230.
23. H.W. Milliman, H. Ishida, DA. Schiraldi, Structure property relationships and the role of processing in the reinforcement of nylon 6-POSS blends. Macromolecules, **45**, 4650 (2012).
24. Kuo P.C.; Sahu D.; Yu H.H. Properties and biodegradability of chitosan/nylon 11 blending films. *Polym Degrad Stabil* **2006**, *91*, 3097.
25. Fornes T.D.; Paul D.R. Modeling properties of nylon 6/clay nanocomposites using composite theories. Polymer, **2003**, *44*, 4993.
26. Li Y.; Huang Z.M.; Lu Y.D. Electrospinning of nylon-6, 66, 1010 terpolymer. *Eur Polym J* **2006**, *42*, 1696.
27. Zheng H.; Du Y.M.; Yu J.H.; Huang R.H.; Zhang L.N.; Preparation and characterization of chitosan/poly(vinyl alcohol) blend fibers. *J Appl Polym Sci* **2001**, *80*, 2558.
28. Wan Y.; Wu H.; Yu A.X.; Wen D.J. Biodegradable polylactide/chitosan blend membranes. *Biomacromolecules* **2006**, *7*, 1362.

Figure legends

Figure 1 Microstructure of OA-POSS (a) and PGN (b).

Figure 2 POM images for PA6/CS blends. Weight ratio of PA6 to CS: a) 50:50; b) 75:35; c) 95:5. The magnification is 10 times.

Figure 3 POM images for a) PA6/CS blends and PA6/CS with 2 wt% nanofiller: b) PA6/CS-POSS; c) PA6/CS-PGN; d) PA6/CS-TCN; e) PA6/CS-TL. The magnification is 10 times.

Figure 4 XRD spectra of PA6/CS and its nanocomposites with different nanofillers.

Figure 5 TEM imgaes for polymer nanocomposites: a) PA6/CS-POSS; b) PA6/CS-PGN; c) PA6/CS-TCN; d) PA6/CS-TL.

Figure 6 a) DSC thermograms of PA6/CS nanocomposites during first heating scan, b) DSC thermograms of PA6/CS nanocomposites during cooling scan.

Figure 7 Tensile strength and breaking strains of CS, PA6, PA6/CS and PA6/CS nanocomposites. Data are expressed as the means ± SD, n=5.

Figure 8 SEM images of PA6/CS and PA6/CS nanocomposites. x) denotes the SEM images of top side; x') assigns the SEM images of bottom side. a) PA6/CS; b) PA6/CS-PGN; c) PA6/CS-TCN; d) PA6/CS-TL; e) PA6/CS-POSS.

Figure 9 SEM images of the cross-section of PA6/CS and PA6/CS nanocomposites. a) PA6/CS; b) PA6/CS-PGN; c) PA6/CS-TCN; d) PA6/CS-TL; e) PA6/CS-POSS.

Figure 10 ATR spectra of PA6/CS and PA6/CS nanocomposites. a) top side; b) bottom side.

Figure 11 Typical selected zone for EDX (The sample is PA6/CS-POSS

nanocomposites). a) cross-section upper zone; b) cross-section middle zone; c) cross-section lower zone; d) top side; e) bottom side.

Figure 12 Proposed mechanism of the influence of migration of nanofiller to the tensile strength.

Tables

Table 1 DSC results of PA6/CS and PA6/CS nanocomposites

	T_m^1°C	T_c^1°C	ΔH_m^1J/g	ΔH_c^1J/g
PA6/CS	220.4	183.7	28.7	25.8
PA6/CS-POSS	221.3	187.6	30.4	28.3
PA6/CS-PGN	221.0	187.4	24.1	22.4
PA6/CS-TCN	221.1	186.0	26.4	26.3
PA6/CS-TL	221.2	185.9	27.1	18.7

Table 2 Silicon atoms content of PA6/CS and PA6/CS nanocomposites.

Samples	Cross-section upper zone	Cross-section middle zone	Cross-section lower zone	Top side	Bottom side
PA6/CS-POSS	0.68	0.37	0.04	0.26	0.12
PA6/CS-PGN	0.08	0.10	0.22	0.08	0.23
PA6/CS-TCN	0.15	0.11	0.33	0.26	0.38
PA6/CS-TL	0.10	0.15	0.49	0.19	0.45

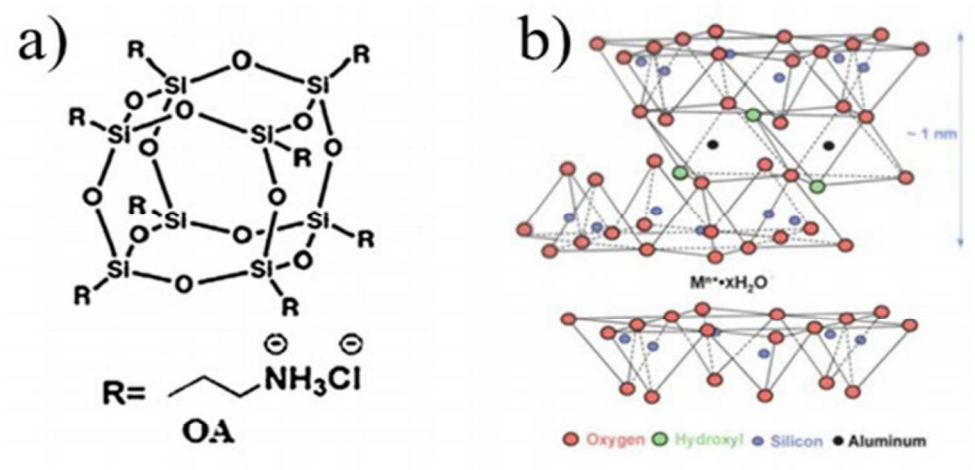

Figure 1

204x107mm (300 x 300 DPI)

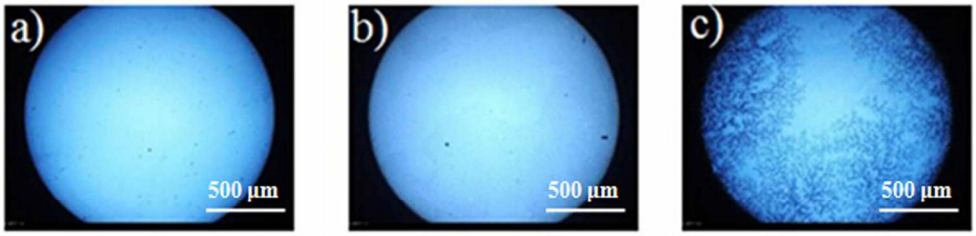

Figure 2

162x51mm (300 x 300 DPI)

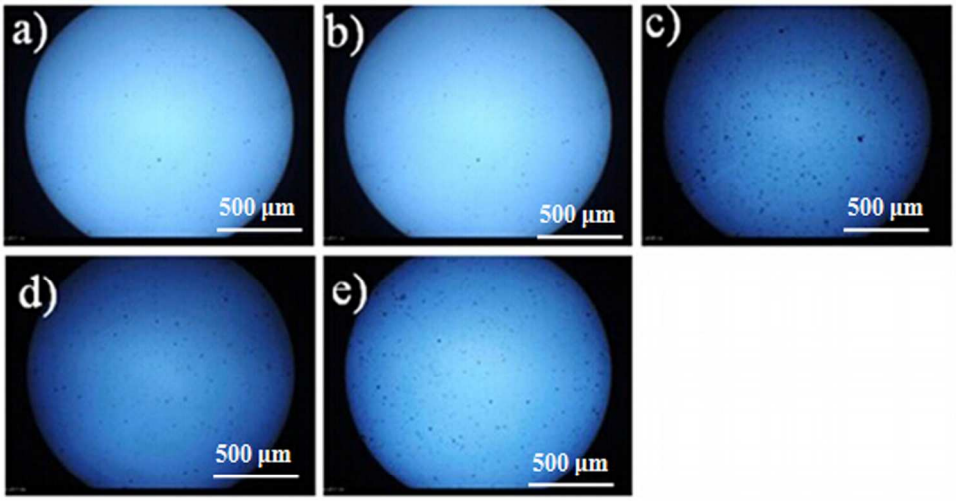

Figure 3

150x87mm (300 x 300 DPI)

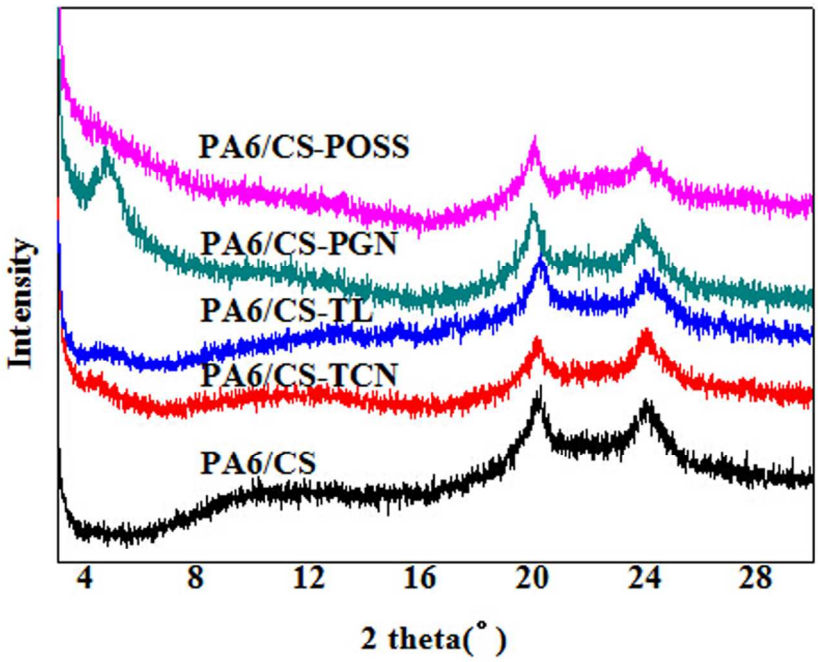

Figure 4

138x104mm (300 x 300 DPI)

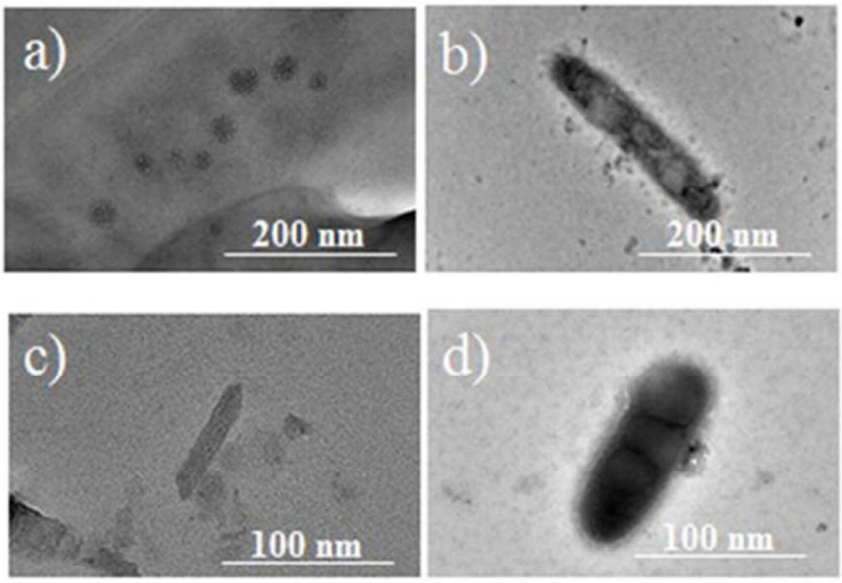

Figure 5

174x116mm (300 x 300 DPI)

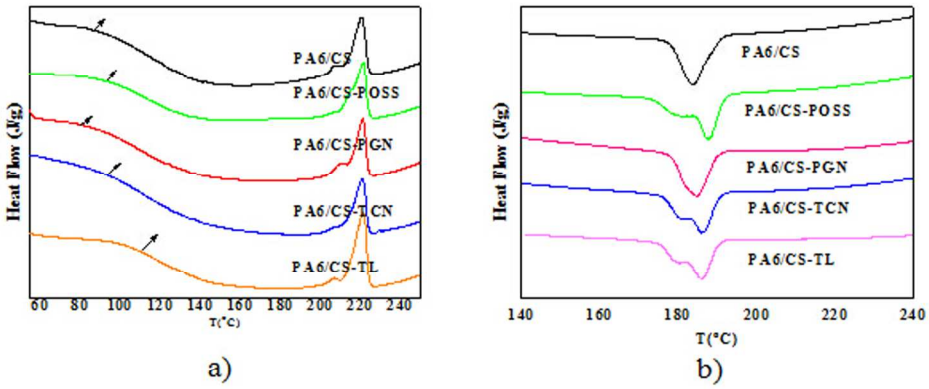

Figure 6

166x81mm (300 x 300 DPI)

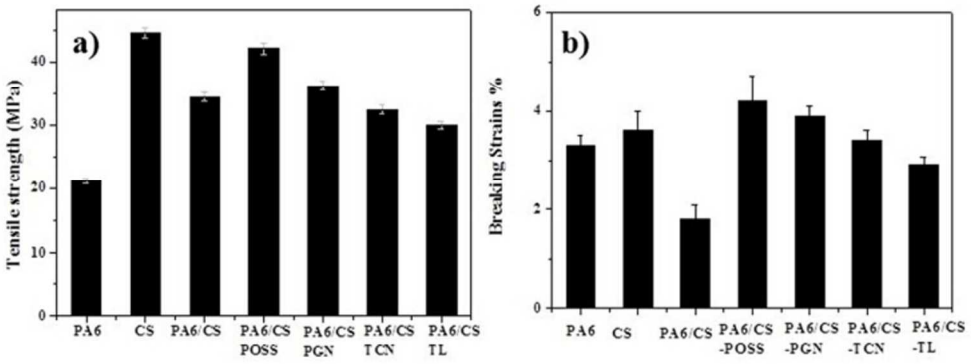

Figure 7

197x91mm (300 x 300 DPI)

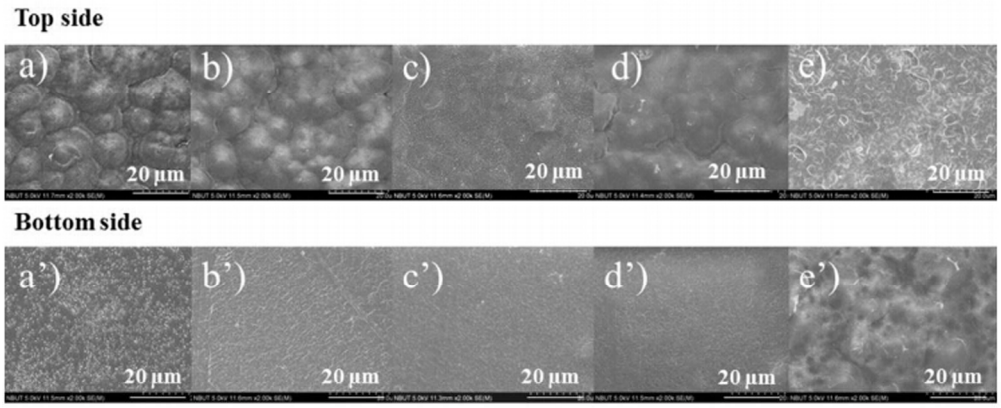

Figure 8

197x94mm (300 x 300 DPI)

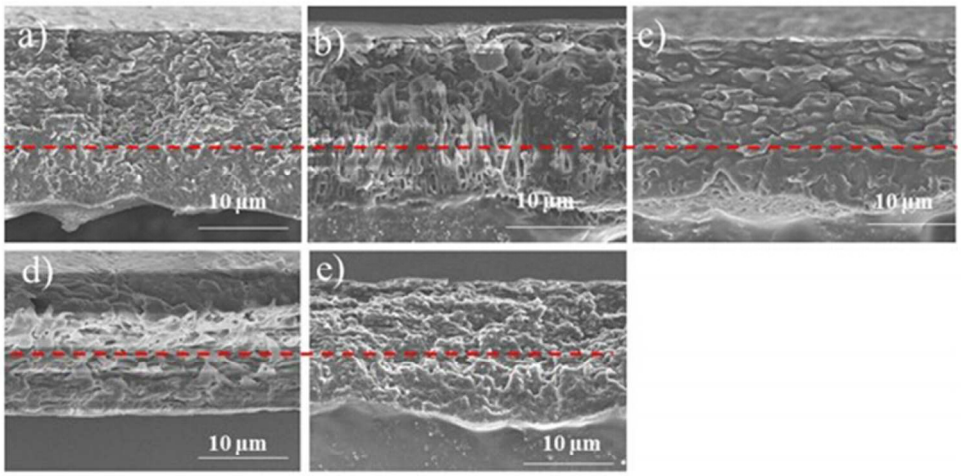

Figure 9

202x113mm (300 x 300 DPI)

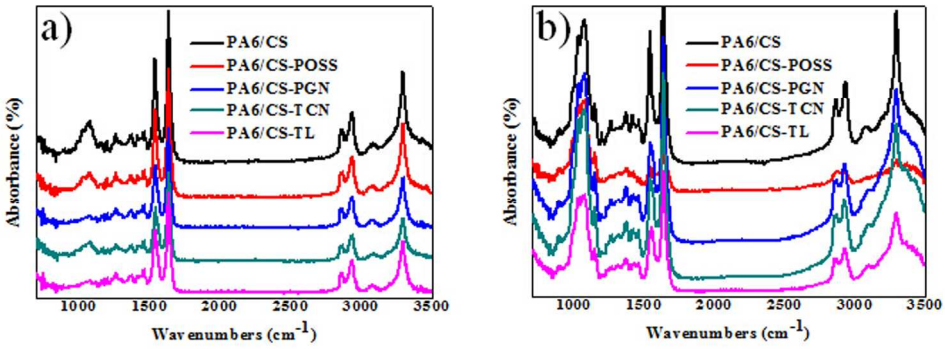

Figure 10

186x76mm (300 x 300 DPI)

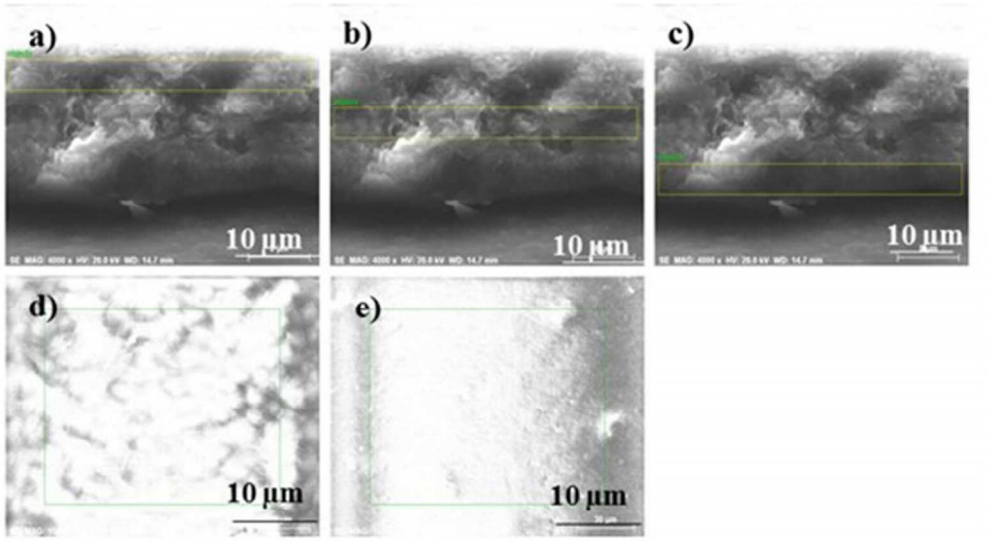

Figure 11

195x119mm (300 x 300 DPI)

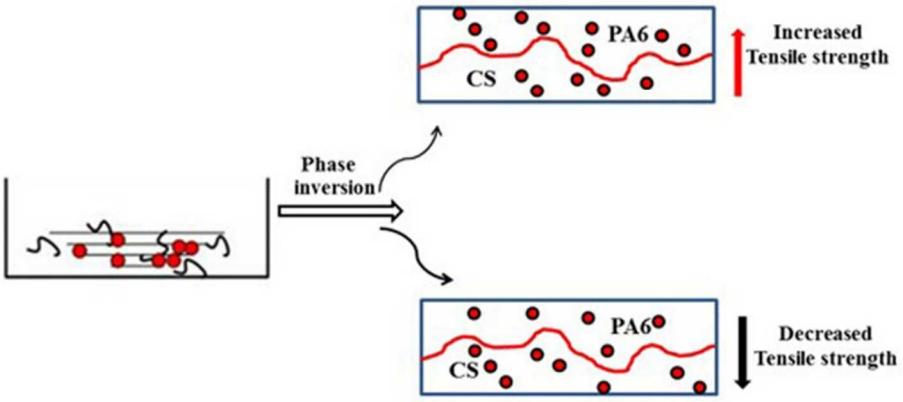

Figure 12

203x108mm (300 x 300 DPI)

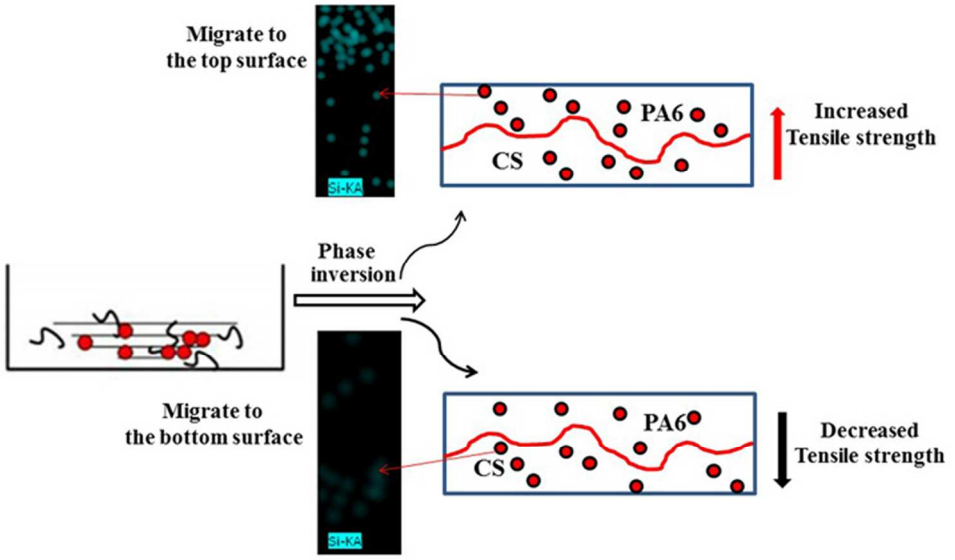

Graphic abstract

198x128mm (300 x 300 DPI)